NONLINEAR FE ANALYSIS ON THE STATIC BUCKLING BEHAVIOR OF THE SPACER GRID STRUCTURES

*K-N SONG**

Korea Atomic Energy Research Institute
150 Dukjin-dong, Yusong-go, Taejon 305-353, Korea
Phone: +82-42-868-2254, Fax: +82-42-863-0565
E-mail*: knsong@nanum.kaeri.re.kr

K-H YOON , KAERI

Korea Atomic Energy Research Institute
150 Dukjin-dong, Yusong-go, Taejon 305-353, Korea
Phone: +82-42-868-8918, Fax: +82-42-863-0565
E-mail: khyoon@nanum.kaeri.re.kr

Key Words: Simulation-Non-linear-Structural

In this study considered is the static buckling behavior of spacer grids in the fuel assembly, which are required to have a sufficient strength against an accident like earthquake. Special attention is given to the finite element modeling of the spot-welding and the constraints between the spacer strips assembled together: it is found that a proper treatment of the constraints is critical for accurate assessment of the buckling behavior including strain localization at the point of spot welding. The buckling strength of the 17x17 spacer grid, which is difficult to analyze due to a large number of degrees of freedom, is estimated from analysis for the smaller models 3x3, 5x5, 7x7, and 9x9 spacer grids.

INTRODUCTION

The spacer grids constitute the primary fuel assembly structural elements of the pressurized water reactor. Each grid is an interconnected array of slotted grid straps that are interconnected and brazed or welded at the intersections to form an egg crate structure. Structural grids support and align the fuel rods, mix the coolant in the high heat transfer core regions, guide the fuel assemblies past each other during handling and, if need be, sustain seismic loads. The structure grids, such as the one illustrated in Figure 1 support the fuel rods both laterally and axially with a friction grip. The fuel assembly incorporates from seven to eleven structural grids, which are made from Inconel 718 or Zircaloy.

One of the most important roles of the spacer grid is to protect the fuel assembly from the unexpected extreme load caused by for example, an earthquake. It is therefore necessary for the grids to have sufficient strength against buckling loads, and the static analysis of the buckling behavior is hence an important element in

the structural design of the spacer grids. To obtain reasonable data of buckling strength and to utilize them in design, at least more than twenty experiments involving the specimens should be performed. However, these experiments require a lot of time and cost because the whole structure of a spacer grid consists of many cells that are welded each other. It is thus getting more and more popular to use computer simulations rather than experiments for the buckling analysis of spacer grids.

In this paper, nonlinear static finite element simulations on the two kinds of spacer grids, one manufactured using single straps and the other manufactured using doublet straps, are performed to investigate their buckling behavior. The detailed geometry of the unit cell of the spacer grid and boundary conditions for the simulation are given in the next section, and they are followed by the simulation results of buckling behavior and deformed shape of the unit cell. Next the simulation is extended to 3x3 cells, and the results are comprehensively compared with experiments. The 5x5 and 7x7 cells are also simulated. Then the tendency of the change in buckling load as the number of cells increases is investigated, and the prediction of the buckling load of the full size spacer grid having 17x17 cells is provided.

THEORETICAL BACKGROUND

Linear and Nonlinear Buckling Analysis

Some buckling modes and buckled shapes could be expected through the buckling eigenvalue analysis by linear buckling analysis, expecting the bifurcation load for the structure. The linear analysis, as the precedent for the nonlinear analysis, is used to investigate the sensitivity on the defects of the structure. The stiffened structures are considered as the structure that has large stiffness and deforms a little just before the buckling occurs. The stiffened structures also have the characteristics to respond strongly loads acting along the principal axis just before the critical buckling load and then to suddenly collapse after the buckling. Linear analysis gives some useful information on the buckling behavior; however, it can't expect the detail post buckling behavior neglecting the deformation of the pre-buckling stage. Therefore in order to understand the buckling behavior of the structure, nonlinear buckling analysis is required.

Governing Equation

The governing equation of the FEM model is expressed as follows:

$$\frac{\partial T_{ij}}{\partial \varsigma_i} + \rho b_j = 0 \quad on \quad V$$
$$T_{ij} n_i = \overline{t_j} \qquad on \quad S_{ij} \qquad \text{(Eq. 1)}$$

Multiply the virtual displacement, ∂u, and integrate by parts

$$\int_V (\frac{\partial(T_{ij}\delta u_j)}{\partial \varsigma_i} - T_{ij}\frac{\partial \delta u_j}{\partial \varsigma_i} + \rho b_j \delta u_j) dV$$
$$= \int_{St_j} \overline{t_j} \delta u_j dS - \int_V T_{ij}\frac{\partial \delta u_j}{\partial \varsigma_i} dV + \int_V \rho b_j \delta u_j dV = 0 \quad \text{(Eq. 2)}$$

From Eq. 2, the governing equation can be expressed as follows:

$$\int_V T_{ij}\frac{\partial \delta u_j}{\partial \varsigma_i} dV = \int_{St_j} \overline{t_j} \delta u_j dS + \int_V \rho b_j \delta u_j dV \quad \text{(Eq. 3)}$$

Not considering the body force using the 2nd PK stress and in the case of undeformed configuration, Eq. 3 can be expressed as follows:

$$\int_{V^0} S_{IJ}\frac{\partial x_I}{\partial X_J}\frac{\partial \delta u_I}{\partial X_I} dV = \int_{St_I^0} \overline{t_I^0} \delta u_j dS \quad \text{(Eq. 4)}$$

Using the shape function, the virtual displacement, ∂u can be approximated as follows:

$$\delta u_k = \sum_{\alpha}^{m_k} N^\alpha d_k^\alpha \qquad and \quad \delta u_k = 0 \quad on \quad S_{u_k}^0 \quad \text{(Eq. 5)}$$

where α and m_k are the nodal number and the number of free nodes of $V^0 - S_u^0$, respectively. And d_k is the displacement at node *k*, and N is the shape function.

Insert Eq. 5 into Eq. 4,

$$\sum_{\alpha}^{m_I} d_I^\alpha \left[\int_{V^0} S_{IJ}\frac{\partial x_I}{\partial X_J}\frac{\partial N^\alpha}{\partial X_I} dV - \int_{St_I^0} \overline{t_I^0} N^\alpha dS \right] = 0 \quad \text{(Eq. 6)}$$

Using the global degree of freedom, Eq. 6 can be expressed as follows:

$$\int_{V^0} S_{IJ}\frac{\partial x_I}{\partial X_J}\frac{\partial N^\alpha}{\partial X_I} dV - \int_{St_I^0} \overline{t_I^0} N^\alpha dS = F_L(q^\beta) - p_L = 0 \quad \text{(Eq. 7)}$$

Above equation can be expressed using the vector notation as follows:

$$F(q^\beta) - p = 0 \quad \text{(Eq. 8)}$$

where *q* denotes the nodal displacement vector and *p* denotes the nodal force relating external force, and *F* denotes the nodal force corresponding the internal stresses.

Applying the Newton method, Eq. (8) can be expressed at the *i+1th* as follows:

$$F(q^{\beta(n,i)}) - p^{(n,i+1)} + \left(\frac{\partial F}{\partial q^{\beta}}\right)^{(n,i)} \Delta q^{\beta(n,i+1)} = 0 \qquad \text{(Eq. 9)}$$

The Jacobian matrix, $\left(\frac{\partial F}{\partial q^{\beta}}\right)^{(n,i)}$ can be expressed as follows:

$$\begin{aligned} & e_L \cdot \left(\frac{\partial F}{\partial q^{\beta}}\right)^{(n,i)} \cdot \Delta q^{\beta(n,i+1)} = (\Delta F_L)^{(n,i)} \\ & = \int_{V^0} \left[\Delta S_{IJ}^{(n,i+1)} \frac{\partial x_l}{\partial X_J} \frac{\partial N^{\alpha}}{\partial X_I} + S_{IJ} \frac{\partial \Delta x_l^{(n,i+1)}}{\partial X_J} \frac{\partial N^{\alpha}}{\partial X_I} \right]^{(n,i)} dV \end{aligned} \qquad \text{(Eq. 10)}$$

The 2nd P-K stress can be expressed as follows:

$$S_{IJ} = C_{IJKL} E_{KL} = \frac{1}{2} C_{IJKL} \left(\frac{\partial x_l}{\partial X_K} \frac{\partial x_l}{\partial X_L} - \delta_{KL} \right) \qquad \text{(Eq. 11)}$$

$$\Delta S_{IJ} = C_{IJKL} \Delta E_{KL} = C_{IJKL} \frac{\partial x_l}{\partial X_K} \frac{\partial x_l}{\partial X_L} \qquad (\because C_{IJKL} = C_{IJLK})$$

Insert Eq. 11 into Eq. 10,

$$\begin{aligned} (\Delta F_L)^{(n,i)} &= \int_{V^0} \left[\frac{\partial N^{\alpha}}{\partial X_I} \frac{\partial x_a}{\partial X_J} C_{IJKL} \frac{\partial x_a}{\partial X_K} \frac{\partial \Delta x_a^{(n,i+1)}}{\partial X_L} + \frac{\partial N^{\alpha}}{\partial X_I} S_{IJ} \frac{\partial \Delta x_l^{(n,i+1)}}{\partial X_L} \right]^{(n,i)} dV \\ &= \sum_{\beta}^{m_{\alpha}} \int_{V^0} \left\{ \frac{\partial N^{\alpha}}{\partial X_I} \frac{\partial x_l}{\partial X_J} C_{IJKL} \frac{\partial x_a}{\partial X_K} \frac{\partial N^{\beta}}{\partial X_L} \right\} dV \, \Delta q_a^{\beta(n,i+1)} \\ &= \sum_{\beta}^{m_l} \int_{V^0} \left\{ \delta_{al} \frac{\partial N^{\alpha}}{\partial X_I} S_{IJ} \frac{\partial N^{\beta}}{\partial X_L} \right\}^{(n,i)} dV \, \Delta q_a^{\beta(n,i+1)} \end{aligned} \qquad \text{(Eq. 12)}$$

Rewriting Eq. 9 in the global degree of freedom

$$K_{LJ}^{t(n,i)} \, \Delta c_J^{(n,i+1)} = p_L^{(n,i+1)} - F_L^{(n,i)} \qquad \text{(Eq. 13)}$$

Stiffness matrix can be obtained from Eq. (12) and Eq. (13) as follows:

$$\begin{aligned} K_{LJ}^{t(n,i)} &= \int_{V^0} \left\{ \frac{\partial N^{\alpha}}{\partial X_I} \frac{\partial x_l}{\partial X_J} C_{IJKL} \frac{\partial x_j}{\partial X_K} \frac{\partial N^{\beta}}{\partial X_L} \right\}^{(n,i)} dV + \int_{V^0} \left\{ \delta_{jl} \frac{\partial N^{\alpha}}{\partial X_I} S_{IJ} \frac{\partial N^{\beta}}{\partial X_L} \right\}^{(n,i)} dV \\ &= K_{LJ}^{(0)(n,i)} + K_{LJ}^{(1)(n,i)} + K_{LJ}^{(2)(n,i)} + K_{LJ}^{(\sigma)(n,i)} \end{aligned} \qquad \text{(Eq. 14)}$$

where $K_{LJ}^{(0)(n,i)} = \int_{V^0} \left\{ \frac{\partial N^\alpha}{\partial X_I} C_{IljL} \frac{\partial N^\beta}{\partial X_L} \right\}^{(n,i)} dV$

$$K_{LJ}^{(1)(n,i)} = \int_{V^0} \left\{ \frac{\partial N^\alpha}{\partial X_I} C_{IlKL} \frac{\partial u_j}{\partial X_K} \frac{\partial N^\beta}{\partial X_L} + \frac{\partial N^\alpha}{\partial X_I} \frac{\partial u_l}{\partial X_J} C_{IJjL} \frac{\partial N^\beta}{\partial X_L} \right\}^{(n,i)} dV$$

$$K_{LJ}^{(2)(n,i)} = \int_{V^0} \left\{ \frac{\partial N^\alpha}{\partial X_I} \frac{\partial u_l}{\partial X_J} C_{IJKL} \frac{\partial u_j}{\partial X_K} \frac{\partial N^\beta}{\partial X_L} \right\}^{(n,i)} dV$$

$$K_{LJ}^{(\sigma)(n,i)} = \int_{V^0} \left\{ \delta_{jl} \frac{\partial N^\alpha}{\partial X_I} S_{IJ} \frac{\partial N^\beta}{\partial X_J} \right\}^{(n,i)} dV$$

Eq. 14 is consisting of four terms, where $K^{(0)}$ is the stiffness from the linear analysis and the other terms are the stiffness from the non-linear analysis.

BUCKLING ANALYSIS

Two kinds of spacer grids are considered as objects for the nonlinear buckling analysis. First, a spacer grid composed of single straps; second, a spacer grid composed of doublet straps. Each spacer grid strap is made from stainless steel (SUS304) whose Young's modulus and Poisson's ratio is 110GPa and 0.3, respectively from the tensile test specimen. Since the simulation is fully nonlinear, the plastic property of the material is also considered as the yield strength is 600Mpa, and the hardening curve by fitting data from tensile tests is employed.

Spacer Grid Composed of Single Straps

FE Models and Boundary Conditions

The geometry and an example of FE modeling for a unit cell of the spacer grid composed of single straps are illustrated in Figure 1. It has 8 dimples and 4 spring parts, which in contact with a fuel rod. The dimension of the primary cube is 12.8 x 12.8 x 35(mm) and the thickness of the strap is 0.6(mm).

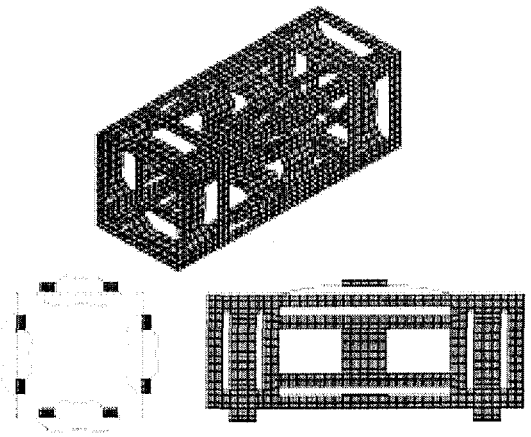

Figure 1. The geometry of unit cell of spacer grid composed of single strap

FE Models and Boundary Conditions

In order to investigate the mesh dependence of the buckling response of the unit cell, three different FE meshes are considered, as given in Figure 2. For all meshes in this paper, 8-node shell elements are employed. The numbers of elements are 392, 556 and 5872, and the number of nodes are 1568, 2156 and 19440, respectively.

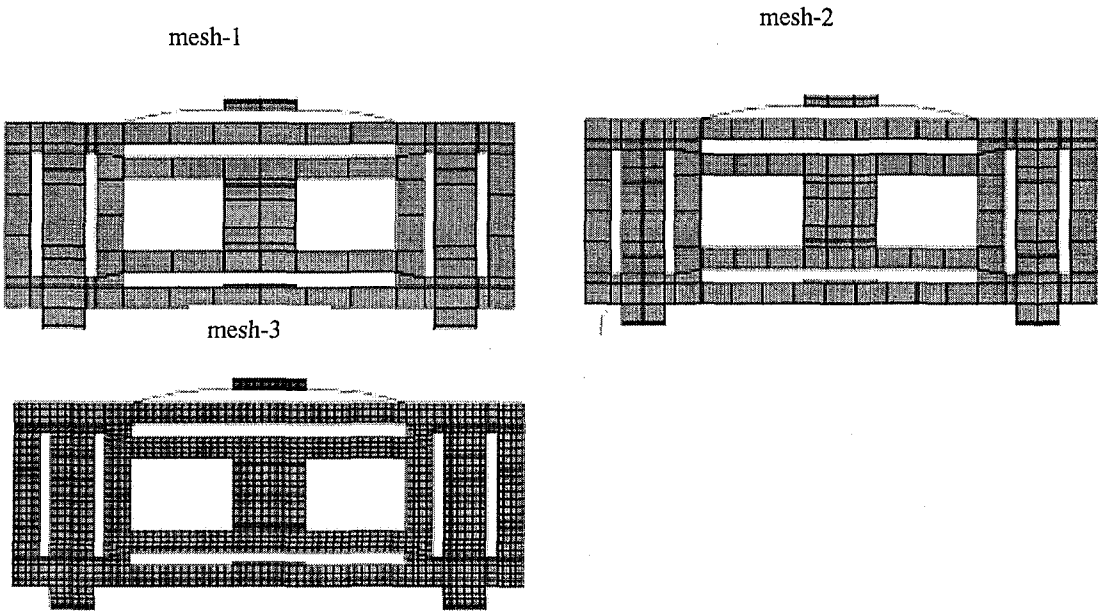

Figure 2. Side-view of three FE meshes

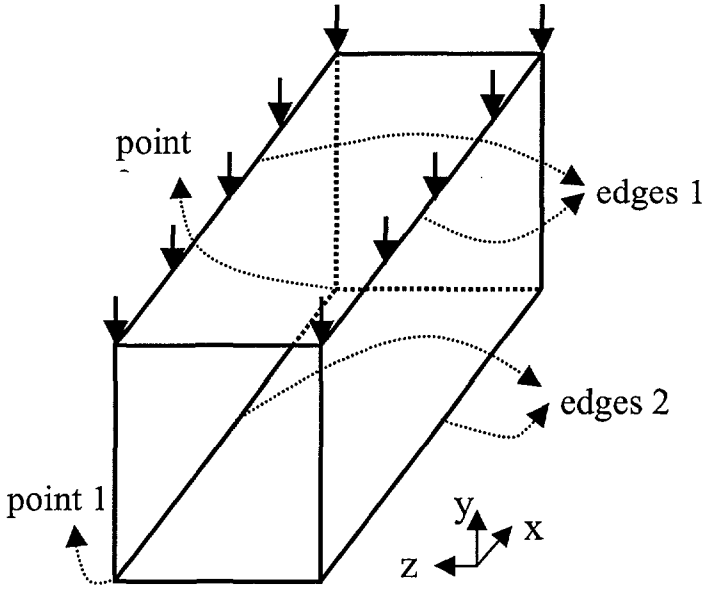

Figure 3. Prescription of boundary conditions

The boundary conditions are well depicted in Figure 3. The corner lines (edges 2) of the lower face are supported and allowed to slide in a z-axis except points 1 and 2, which are prohibited from sliding to prevent the model from rotating. On edges 1, downward displacement conditions are uniformly prescribed to simulate the compression.

Maximum Reaction Forces

For the simulations, the nonlinear analysis of ABAQUS with prescribed essential boundary conditions is used. In designing the spacer grid, the most important structural property regarding buckling is the critical buckling strength under the condition of compression. The displacements vs. total reaction force curves are plotted in Figure 4 for comparing the responses of the different meshes given above. The reaction force is obtained by summing over all nodes on the corner where the prescribed downward displacement boundary condition is imposed. It is shown that each FE model gives similar values of maximum reaction force, about 4.6E+3 ~ 4.7E+3(N). Figure 4 also demonstrates that the behavior of all meshes before reaching maximum reaction force almost coincide with each other, even though the post-buckling behaviors are a little different. The maximum reaction forces of the three kinds of meshes are 4.71E+3, 4.64E+3, and 4.60E+3 N, respectively. From this comparison, it is concluded that the coarse mesh (mesh-1) can be used for the simulation of multi-cell spacer grid, which will be presented in the next section, in order to save computing time with maintaining the accuracy for the maximum reaction force.

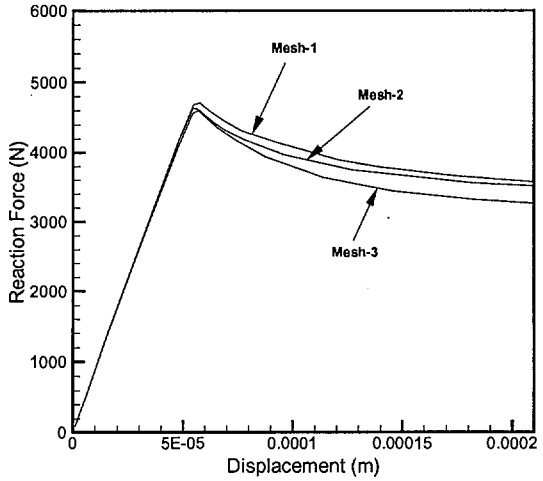

Figure 4. Displacement/reaction force curves of the three meshes

Multi-cell Spacer Grids

In this section, the nonlinear buckling simulations are extended to multi-cell spacer grids. Four kinds of arrays, i.e., 3x3, 5x5, 7x7, and 9x9 array, are considered. The multi-cell grid is made by interconnecting the slotted grid straps and by welding at the interactions. So, we must pay attention to make finite element modeling at the interconnecting parts and the intersections. Considering the geometry at the interconnecting part shown in Figure 5, we use the following constraints.

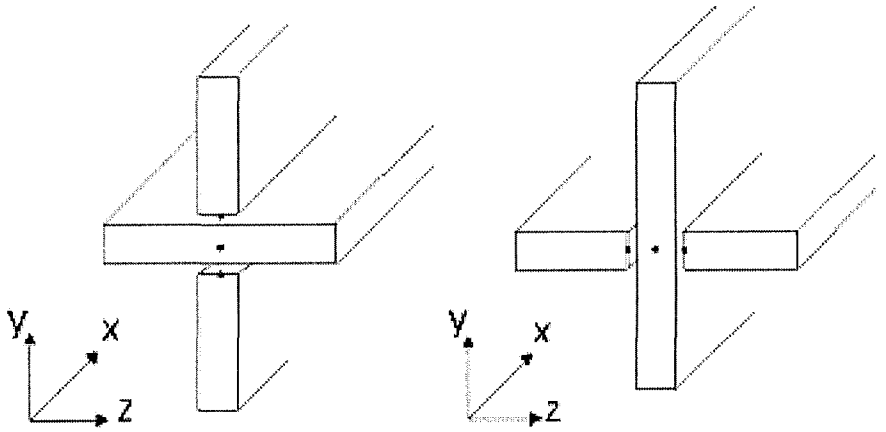

(a) (b)

Figure 5. Restriction at connecting parts between vertical and horizontal plates

1) for Figure 5(a) configuration: restrict the degree of freedom θ_z

2) for Figure 5(b) configuration: restrict the degree of freedoms u_z, θ_x, θ_y

Also at the intersections, instead of using 1-point welding model we use the 6-points welding model, shown in Figure 6, where all of the degree of freedoms at the 6-points are restricted considering the welding nugget size

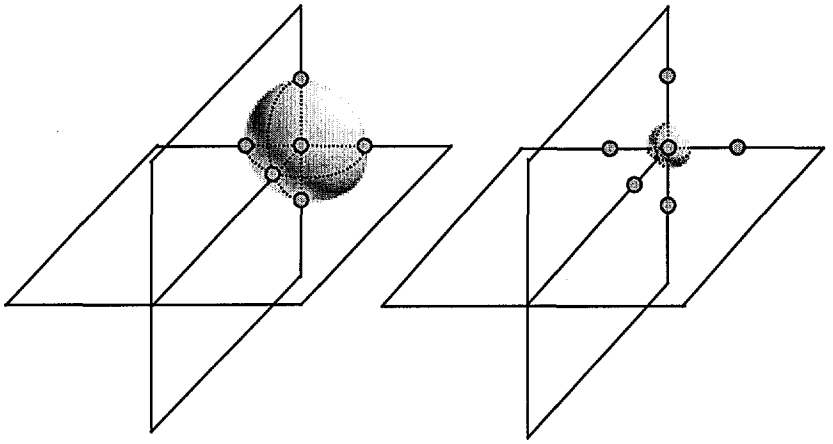

(a) 6 point welding model (b) 1 point welding model

Figure 6. Restriction at connecting parts between vertical and horizontal plates

The boundary conditions are prescribed in similar way for the case of the unit cell in the previous section. For example, the prescribed boundary conditions for 3x3 grid are illustrated in Figure 7.

The maximum reaction force from this 3x3 spacer grid simulation, 4568N, is compared with the values of critical buckling strength obtained from experiment, 4497N. The value from the simulation is slightly less than the maximum value among the experiments. Therefore it can be concluded that the simulation properly predicts the critical buckling strength of the 3x3 grid.

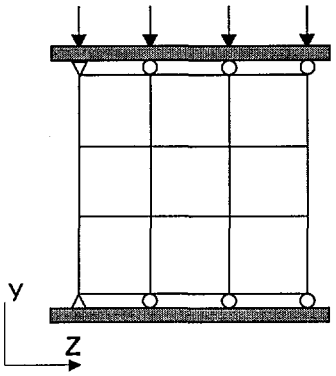

Figure 7. Boundary condition for the simulation of 3x3 spacer grid

It is interesting that the deformation of multi-cell spacer grids occurs mainly on the top and bottom arrays as shown in Figure 8 for 5x5 grid. The other middle layers maintain its original shape. This result is common no matter how many cells of spacer grids are employed. This pattern of deformation is also confirmed by the experiments for 3x3 spacer grids. In conclusion on the deformed shape, the shear-like deformation is concentrated only on the top and bottom layers of cells. Therefore the maximum reaction force is proportional to the number of cells on the top or bottom array. To verify this, the maximum reaction forces for the number of cells are summarized shown in Figure 9. It can easily be shown that a linear equation can approximately be derived from the values of from 3x3 array and to 9x9 array as

$$F_M\left(\times 10^{-3}\right) = 1.04(N-3) + 4.53 \qquad \text{(Eq. 15)}$$

where F_M is the maximum reaction force and N is the number of cells in one layer of the space grid considered. According to the equation, the maximum reaction force of 17x17 array can be predicted to be 19.1kN, and this prediction will be composed with the test result in the future.

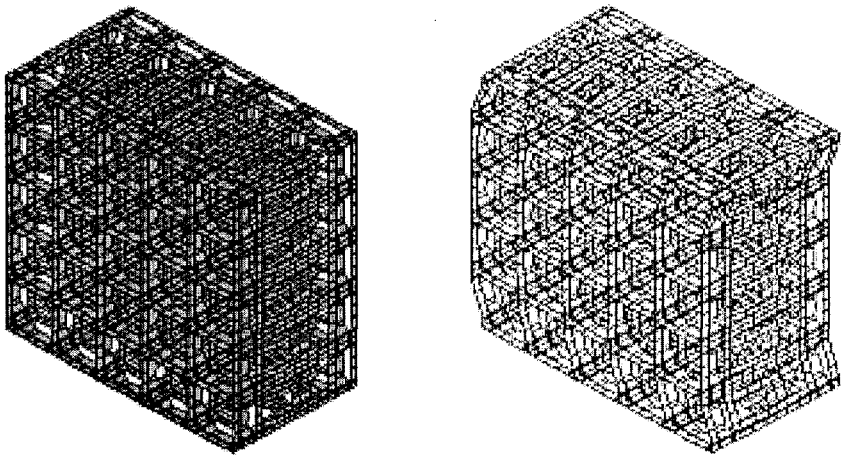
Figure 8. FE mesh and deformed result of 5x5spacer grid

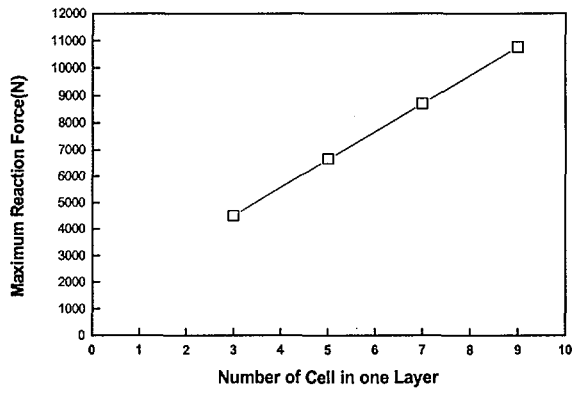

Figure 9. Buckling strength according to number of cells

Spacer Grid Composed of Doublet Straps
FE Models and Boundary Conditions
The geometry and an example of FE modeling for 3x3 array of the spacer grid composed of doublet straps are illustrated in Figure 10. It has 4 line-spring parts, which in contact with a fuel rod in each unit cell. The dimension of the primary cube is 12.8 x 12.8 x 35(mm) and the thickness of the strap is 0.3(mm).

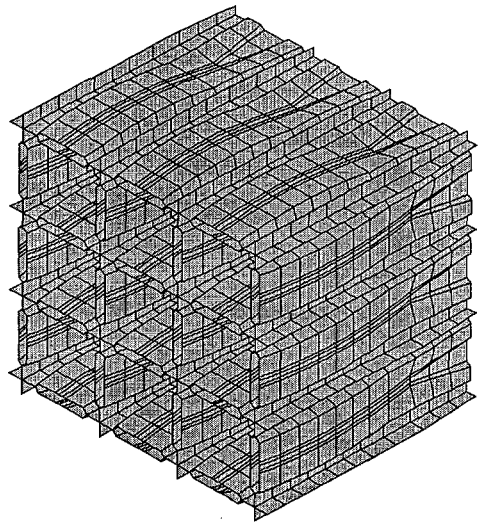

Figure 10. Finite element model of doublet spacer grid

FE Models and Boundary Conditions
In order to investigate the mesh dependence of the buckling response of the unit cell, two different FE meshes are considered. For all meshes in this paper, 8-node shell elements are employed.

Multi-cell Spacer Grids
The maximum reaction force from this 3x3 spacer grid simulation, 2220N, is

compared with the values of critical buckling strength obtained from experiment, 2587N. The value from the simulation is a little less than the maximum value among the experiments. Therefore it can be concluded that the simulation can predict the critical buckling strength of the 3x3 grid.

It is interesting that the deformation of multi-cell spacer grids shown in Figure 11 also occurs mainly on the top and bottom arrays as the same as the spacer composed of single straps. The other middle layers maintain its original shape. This result is common no matter how many cells of spacer grids are employed. This pattern of deformation is also confirmed by the experiments for 3x3 spacer grids. In conclusion on the deformed shape, the shear-like deformation is concentrated only on the top and bottom layers of cells. Therefore the maximum reaction force is proportional to the number of cells on the top or bottom array. To verify this, the maximum reaction forces for the number of cells are summarized shown in Figure 12. It can easily be shown that a linear equation can approximately be derived from the values of from 3x3 array and to 9x9 array as

$$F_M\left(\times 10^{-3}\right) = 0.645(N-3) + 0.209 \qquad \text{(Eq. 16)}$$

where F_M is the maximum reaction force and N is the number of cells in one layer of the space grid considered. According to the equation, the maximum reaction force of 17x17 array can be predicted to be 11.2kN, and this prediction will be compared with the test result in the future.

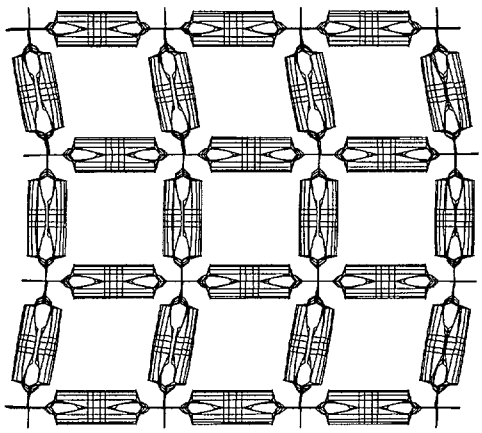

Figure 11. Deformed shape of 3x3 cell

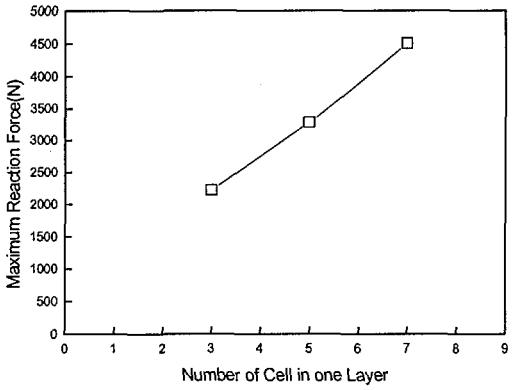

Figure 12. Buckling strength according to number of cells

CONCLUSION AND DISCUSSION

The nonlinear buckling analysis of the spacer grid in fuel assembly was conducted by using the static finite element method. It is noticed that shear collapsing of the grid structures are developed from and confined in the top and bottom layer out of the multi-cell grids, while the middle layers always keep their initial shapes. This pattern of deformation well agrees with the experimental results. It is also verified that the predicted critical buckling strength falls into the range of experimental variations.

The critical buckling strength of multi-cell grids show the trend of linear increases with the number of cells on one face of the grids. From the equation that can empirically be derived from 3x3, 5x5, 7x7, and 9x9 array of spacer grids, it is possible to estimate approximately that the critical buckling strength of the whole structure of a spacer grid, 17x17 cells.

ACKNOWLEDGEMENT

This project has been carried out under the nuclear R&D program by MOST.

REFERENCE

[1] K-H, Choi, S-K, Jun, K-H, Yoon, and K-N, Song, " FE Analysis of Nonlinear Buckling Behavior of a Spacer Grid in Fuel Assembly," SMIRT-15, II-381.
[2] K-N, Song and K-H, Yoon, "Nonlinear FE Analysis on the Static Buckling Behavior of the Spacer Grid Structures," Proc. Of the Korean Nuclear Society Autumn Meeting, 2000.